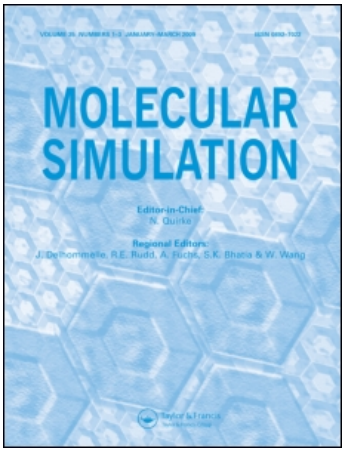

Molecular Simulation
Publication details, including instructions for authors and subscription information:
http://www.informaworld.com/smpp/title~content=t713644482

Modeling Confined Fluids: An NhPT Molecular Dynamics Method

Jee-Ching Wang[a]; Saroja Saroja[a]
[a] Department of Chemical Engineering, University of Missouri-Rolla, Rolla, MO, USA

Online publication date: 26 October 2010

To cite this Article Wang, Jee-Ching and Saroja, Saroja(2003) 'Modeling Confined Fluids: An NhPT Molecular Dynamics Method', Molecular Simulation, 29: 8, 495 — 508
To link to this Article: DOI: 10.1080/0892702031000065575
URL: http://dx.doi.org/10.1080/0892702031000065575

Molecular Simulation, Vol. 29 (8), August 2003, pp. 495–508

Modeling Confined Fluids: An *NhPT* Molecular Dynamics Method

JEE-CHING WANG* and SAROJA SAROJA

Department of Chemical Engineering, University of Missouri-Rolla, Rolla, MO 65409-1230, USA

(Received July 2002; In final form October 2002)

We present an *NhPT* MD method developed for systematic investigation of both the structural and dynamical properties of confined fluids without resorting to chemical potential or explicit reservoir. This method allows confined fluids to expand or contract transversely and the same number of fluid molecules to be simulated throughout all surface separations. Its first implementation using confined Lennard–Jones fluid yields step-like changes in surface density, layered configurations, in-plane ordering, and oscillatory perpendicular pressures and transverse diffusivities that are consistent with previous studies. Additionally, a pseudo-Poisson's ratio and transverse isothermal compressibility were calculated. Like other properties, they oscillate at smaller surface separations and approach constant values when the surface separation becomes sufficiently large. The limiting value of the pseudo-Poisson's ratio is interestingly equivalent to that of incompressible continua.

Keywords: Confined fluids; Molecular dynamics; *NhPT* method; Pseudo-Poisson's ratio; Isothermal compressibility

INTRODUCTION

The behavior of fluids confined to nanometer-scale spaces has stimulated a great deal of interest and effort in recent years. As modern technologies continue to miniaturize devices down to scales comparable to molecular dimensions, the role of these nanoscopically confined fluids (nanoconfined fluids or simply confined fluids) becomes increasingly important and a molecular-level understanding becomes increasingly imperative. Over the past two decades, new experimental techniques, in particular the Surface Force Apparatus (SFA) [1–9], have been able to probe nanoconfined fluids more closely and have revealed many unique properties that are unexpected previously and inexplicable with conventional continuum fluid theories. These properties have been inferred to arise from ordering of confined molecules into configurations not typically found in bulk liquids. Specifically, fluid molecules, induced by confinement, may pack into layers parallel to the confining surfaces. Such layered configurations then cause drastically different structural and dynamical properties from those of corresponding bulk fluids, where molecules are at random. Atomistic computer simulations employing Monte Carlo (MC) [10–14] and molecular dynamics (MD) [14–17] techniques have provided explicit evidences to substantiate the layering behavior of confined fluids. Other theoretical approaches such as density functional theory [18,19] and integral equation theory [20,21] have also been extended to analyze nanoconfined fluids and confirmed the formation of fluid layers under confinement.

Despite our recent success, there are still unsolved discrepancies between experiments and theoretical studies, and unattended issues concerning nanoconfined fluids. Theoretical analyses of structural properties by such methods as density functional and integral equation theories [18–21], and of dynamical properties by such methods as Enskog [22,23] and functional perturbation theories [24–26] have advanced our understanding of nanoconfined fluids. However, their current applications are still limited to simple, idealized systems. Molecular stimulation, on the other hand, can study complex systems and realistic conditions that are more comparable to actual experiments and practical

*Corresponding author. E-mail: jcwang@umr.edu

ISSN 0892-7022 print/ISSN 1029-0435 online © 2003 Taylor & Francis Ltd
DOI: 10.1080/0892702031000065575

applications. It has become, to date, the most preferred theoretical means for the investigation of nanoconfined fluids. Owing to the equilibrium between a confined liquid and its bulk reservoir, their chemical potentials become equal and grand-canonical MC (GCMC) [10–14] has thus been the traditional simulation technique for confined fluids. However, for dense, complex confined systems, GCMC inevitably loses efficiency. Besides, it is a stochastic method not suitable for studying dynamical and transport properties. MD is inherently capable of studying both structural and dynamical properties. Evaluation of chemical potential in MD stimulations has also been achieved recently using virtual test particle methods [27]. It is possible but still rather awkward to directly control chemical potential to a prespecified constant value in MD simulations of confined fluids, especially those of large, complex molecules. Consequently several alternatives have been attempted.

MD simulations have been carried out to study confined liquids by matching the bulk density at the center [28–30] or by fixing the normal load, i.e. normal stress or perpendicular pressure [15,31–34]. However, the former becomes inadequate for very thin confined films and the latter has a limited ability in exploring the full range of properties as a function of surface separation. A more adequate, versatile alternative is to stimulate an isothermal–isobaric liquid droplet [35] or reservoir [17,36] explicitly to which a confined fluid is connected. The tradeoff of this alternative is that it is computationally demanding and likely to suffer slow relaxation between the confined fluid and reservoir and edge effects caused by molecularly finite dimensions of the simulation boxes. These difficulties would become even more pronounced for simulations of large molecules. Winkler *et al.* [37] have attempted to subject confined liquids to constant temperature and constant external pressure to lift the need for chemical potential or fluid reservoir. While conceptually similar to an explicit isothermal–isobaric reservoir, this approach improves computational efficiency and avoids possible shortcomings of slow relaxation and edge effects. Its value is much lessened, however, by such a major drawback that no distinction between the parallel and perpendicular pressures was considered. In fact, fluid molecules adopting anisotropic configurations under confinement result in anisotropic pressures in the parallel and perpendicular directions, which is the origin of solvation force measured by SFA. This pressure anisotropy was embraced in a *NAPT* ensemble method proposed very recently by Wang *et al.* [38,39]. The produced results are consistent with those from GCMC studies and serve to legitimize the *NAPT* method for the study of nanoconfined fluids.

The essence of the *NAPT* ensemble method is to constrain the temperature T and the pressure (or stress) parallel to the confining surfaces $P_{\|}$ to fixed values to define the thermodynamic state of or provide a virtual equilibrium reservoir for a confined fluid (cf. Fig. 1a). This is an accurate representation when the confining surfaces are planar [40,41] and an excellent approximation when the confining surfaces curve extremely slowly as in a SFA from a molecular perspective [40]. According to the virial theorem [42], the instantaneous pressure of a simple confined fluid along the parallel (x and y) directions can be calculated as

$$P_{\|}=\frac{1}{2(Ah)}\sum_{\lambda=x,y}\left[\sum_i\left(\mathbf{p}_i^{\lambda}\cdot\mathbf{p}_i^{\lambda}\right)/m_i + \frac{1}{2}\sum_i\sum_{j\neq i}\mathbf{f}_{ij}^{\lambda}\cdot\mathbf{r}_{ij}^{\lambda}+\sum_i\sum_s\mathbf{f}_{is}^{\lambda}\cdot\mathbf{r}_{is}^{\lambda}\right], \tag{1}$$

where m_i and $\mathbf{p}_i$ are the mass and momentum of a fluid atom, $\mathbf{r}_{ij}=\mathbf{r}_i-\mathbf{r}_j$, $\mathbf{r}_{is}=\mathbf{r}_i-\mathbf{r}_s$, and $\mathbf{f}_{ij}$, $\mathbf{f}_{is}$ are the interaction forces between a pair of atoms separated by $\mathbf{r}_{ij}$ and $\mathbf{r}_{is}$. Superscript λ denotes the projection of vectors onto the x–y plane and subscript s represents the two confining substrates, both having the same surface A and separated by a distance of h in the z direction. $P_{\|}=(P_{xx}+P_{yy})/2$ has been used in Eq. (1) on the account that the system is isotropic in the two parallel directions. Practically, $P_{\|}$ can be constrained by adjusting either h and z coordinates accordingly or A and xy coordinates accordingly, rendering two routes to control the parallel pressure. For MD simulations employing atomically structured substrates, the h route appears more straightforward and was therefore adopted in the *NAPT* method. As a result, h fluctuates constantly during the course of an *NAPT* MD simulation, but its time average converges to a specific value consequent on the pressure constraint. For this *NAPT* method and other simulation techniques employing the same set of confining substrates throughout all separations, the number of confined molecules N naturally decreases with decreasing h and could become rather small at small separations. This may raise a concern of inconsistency or finite-size effects in the simulation results and can make the methods inadequate for simulating large molecules such as polymers and biomolecules. In this work, we developed a new MD simulation method for confined fluids, which overcomes the difficulty of controlling $P_{\|}$ via adjusting A differentially and eliminates the concerns associated with the *NAPT* and other methods. As will be described below, this method can be reasonably termed as an *NhPT* MD method. We introduce this method here and present the results from its first

implementation using Lennard–Jones (LJ) fluids. It is believed that the *NhPT* method is a more adequate, better-equipped simulation method for studying confined fluids, in particular those containing large, complex molecules.

MODELS AND METHOD

Figure 1 displays a simple depiction of a confined fluid between two solid substrates and a schematic of the model system considered in this work. We modeled the fluid atoms and substrate atoms as identical LJ particles, with the latter fixed to their equilibrium bulk positions. The LJ 12-6 potential, truncated and corrected at $r_c = 3.5\sigma$, was used to describe the interatomic interactions. Each confining substrate was represented by five layers of atoms arranged in a face-centered cubic (fcc) lattice having a lattice constant l of 1.5985σ. The confining surfaces are fcc(100) planes placed in registry (cf. Fig. 1b). Periodic boundary conditions are applied in the x and y directions to make the confined systems infinite transversely. Their implementation, however, calls for a special treatment because $P_{\|}$ was intended to be controlled by instantaneous, differential adjustment of the transverse dimensions and coordinates. Adding or eliminating one row of substrate atoms causes a finite, not a differential, dimension change. Varying the interrow spacing between substrate atoms can yield differential changes, but also undesirably alter the crystalline structure of the substrates. To resolve this difficulty, we applied periodic boundary conditions only to the fluid and used a special scheme to construct infinite substrates. Since crystalline substrates possess periodic structures and consist of repetitive unit cells, each fluid atom can be associated with a substrate unit cell characterized by $(n\mathbf{a}_1, m\mathbf{a}_2)$, where $\mathbf{a}_1$, $\mathbf{a}_2$ are known vectors defining the shape and lateral dimensions of a unit cell and n, m are integers or zero. From a simulation point of view, a fluid atom interacts in effect with infinite substrates as long as it "sees" all the substrate atoms within its potential cutoff. We took advantage of these facts and gave each fluid atom infinite substrates by providing blocks of substrate unit cells centered around its characteristic $(n\mathbf{a}_1, m\mathbf{a}_2)$. Neighbor lists of substrate atoms became no longer needed and handling of fluid transverse expansion became straightforward. It worked perfectly for our simulations where the system sizes not only changed constantly at

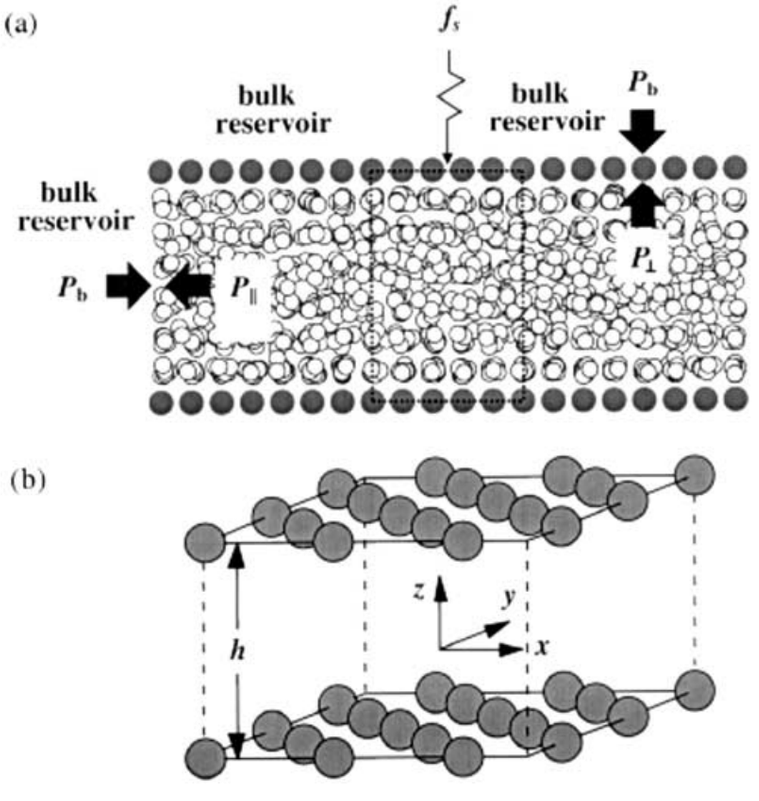

FIGURE 1 (a) Depiction of a confined fluid between two planner substrates immersed in a reservoir under the consideration of *NAPT* and *NhPT* methods. Dashed square signifies a simulation box. (b) Schematic of the model confined system with in-registry substrates and the coordinate system. h is the surface separation.

a fixed h but also underwent sudden, significant expansion due to pressure constraint.

Since the parallel pressure constraint is engaged in the x and y directions, the equations of motion in the two directions take on the *NPT* form [38,39,42],

$$\dot{\mathbf{r}}_i^\lambda = \mathbf{p}_i^\lambda/m_i + \chi(\mathbf{r},\mathbf{p})\mathbf{r}_i^\lambda, \tag{2}$$

$$\dot{\mathbf{p}}_i^\lambda = \mathbf{f}_i^\lambda - \chi(\mathbf{r},\mathbf{p})\mathbf{p}_i^\lambda - \xi_\parallel(\mathbf{r},\mathbf{p})\mathbf{p}_i^\lambda, \tag{3}$$

$$\dot{S}_\lambda = \chi(\mathbf{r},\mathbf{p})S_\lambda, \tag{4}$$

where $\lambda = x$ or y and S_λ signifies the transverse dimensions of a simulation box. $\chi(\mathbf{r},\mathbf{p})$ is a dilation coefficient used to adjust S_λ, i.e. A, to achieve constant parallel pressure. In order not to involve further complexity, we set $S_x = S_y$ and use a common χ to retain the square shape of the simulation boxes. In the perpendicular z direction, the equations of motion assume the *NVT* form,

$$\dot{\mathbf{r}}_i^z = \mathbf{p}_i^z/m_i, \tag{5}$$

$$\dot{\mathbf{p}}_i^z = \mathbf{f}_i^z - \xi_\perp(\mathbf{r},\mathbf{p})\mathbf{p}_i^z. \tag{6}$$

$\xi_\parallel(\mathbf{r},\mathbf{p})$ and $\xi_\perp(\mathbf{r},\mathbf{p})$ are friction coefficients for temperature control, evaluated using Gaussian least-constraint method [42].

Understandably, proper evaluation of χ determines the success of the intended pressure control and thus the success of the *NhPT* method. Previous *NAPT* MD study [39] has shown that the loose coupling method of Berendsen *et al.* [42,43] provides a robust, reliable way to constrain $P_\parallel$ for confined fluids. The change of parallel pressure with time is made by this method to obey $\dot{P}_\parallel = (P_{\parallel,\mathrm{set}} - P_\parallel)/t_p$, where t_p is a coupling time constant. On the other hand, $P_\parallel$ can also be adjusted instantaneously through the rescaling of transverse dimensions and coordinates. Specifically,

$$\dot{P}_\parallel = \frac{\partial P_\parallel}{\partial S_x}\frac{\mathrm{d}S_x}{\mathrm{d}t} + \frac{\partial P_\parallel}{\partial S_y}\frac{\mathrm{d}S_y}{\mathrm{d}t}. \tag{7}$$

With $P_\parallel = (P_{xx} + P_{yy})/2$ and Eq. (4), we can arrive at

$$\dot{P}_\parallel = \frac{\chi}{2}\left(\frac{\partial P_{xx}}{\partial S_x}S_x + \frac{\partial P_{xx}}{\partial S_y}S_y + \frac{\partial P_{yy}}{\partial S_x}S_x + \frac{\partial P_{yy}}{\partial S_y}S_y\right), \tag{8}$$

or

$$\dot{P}_\parallel = -\frac{\chi}{2}\left(\frac{1}{\kappa_{xx}} + \frac{1}{\kappa_{yx}} + \frac{1}{\kappa_{xy}} + \frac{1}{\kappa_{yy}}\right) = -\frac{2\chi}{\kappa_\parallel}, \tag{9}$$

where we have used the following notations,

$$\kappa_{ij} = -(1/S_i)(\partial S_i/\partial P_{jj})_{S_j,h,T}, \tag{10}$$

$$\kappa_\parallel = -(1/A)(\partial A/\partial P_\parallel)_{h,T}. \tag{11}$$

The dilation coefficient for parallel-pressure control can then be evaluated as

$$\chi = -\frac{\kappa_\parallel(P_{\parallel,\mathrm{set}} - P_\parallel)}{2t_P}. \tag{12}$$

$\kappa_\parallel$ and κ_{ij} are instantaneous isothermal compressibilities of a confined fluid at a fixed surface separation under different specifications. We have derived a microscopic expression for $\kappa_\parallel$ as

$$\frac{1}{\kappa_\parallel} = P_\parallel - \frac{1}{4V}\left\{\frac{1}{2}\sum_i\sum_{j\neq i}\left[\frac{X(r_{ij})}{r_{ij}^4}\left(\mathbf{r}_{ij}^\lambda\cdot\mathbf{r}_{ij}^\lambda\right) - \frac{2}{r_{ij}}\frac{\mathrm{d}U}{\mathrm{d}r}\right]\left(\mathbf{r}_{ij}^\lambda\cdot\mathbf{r}_{ij}^\lambda\right)\right.$$
$$\left. + \sum_i\sum_s\left[\frac{X(r_{is})}{r_{is}^4}\left(\mathbf{r}_{is}^\lambda\cdot\mathbf{r}_{is}^\lambda\right) - \frac{2}{r_{is}}\frac{\mathrm{d}U}{\mathrm{d}r}\right]\left(\mathbf{r}_{is}^\lambda\cdot\mathbf{r}_i^\lambda\right)\right\}, \tag{13}$$

where $V = S_xS_yh$ is the volume of the simulation box and $\mathbf{r}^\lambda\cdot\mathbf{r}^\lambda = \mathbf{r}^x\cdot\mathbf{r}^x + \mathbf{r}^x\cdot\mathbf{r}^x$. Detailed derivation and expressions for κ_{ij} and $X(r)$ are provided in Appendix I.

In the *NhPT* method, the instantaneous perpendicular pressure $P_\perp$ along the z direction is left to be measured as in SFA experiments. In contrast to $P_\parallel$, there are more than one formulation available for $P_\perp$, due to the molecularly finite dimensions in this direction. From a mechanical perspective,

$$P_\perp = \frac{1}{2A}\sum_i\sum_s|f_{is}^z|, \tag{14}$$

where f_{is}^z is the scalar force in the z direction between a fluid atom and a substrate and $2A$ results from two confining substrates. From a hydrodynamic perspective, the so-called Method of Plan [44] can be derived to calculate the local perpendicular pressure $P_\perp(z)$ in a confined film. We integrated this $P_\perp(z)$ over the entire confined film to get a tensorial form similar to $P_\parallel$ in Eq. (1),

$$P_\perp = \frac{1}{Ah}\left[\sum_i(\mathbf{p}_i^z\cdot\mathbf{p}_i^z)/m_i + \frac{1}{2}\sum_i\sum_{j\neq i}\mathbf{f}_{ij}^z\cdot\mathbf{r}_{ij}^z\right.$$
$$\left. + \sum_i\sum_s\mathbf{f}_{is}^z\cdot\left(\mathbf{r}_i^z \pm \frac{h}{2}\right)\right], \tag{15}$$

where $-h/2$ is for the top confining substrate located at $z = h/2$ and $+h/2$ is for the bottom one at $z = -h/2$. $\mathbf{p}_i^z$, $\mathbf{f}_{ij}^z$, $\mathbf{r}_{ij}^z$, $\mathbf{f}_{is}^z$, and $\mathbf{r}_i^z$ are projections of the original vectors in the z direction. It is worth noting that both formulations were used and produced the same $\langle P_\perp\rangle$ within statistical errors for every confined film simulated in this project. $<\cdots>$ represents an ensemble average over a phase-space trajectory. In the *NhPT* method, the equilibrium between a confined fluid and its reservoir is represented by

such constraints as $\langle P_{\parallel} \rangle = P_b$ and $\langle T \rangle = T_b$, where P_b and T_b are reservoir pressure and temperature. The solvation force per unit area f_s, a counteracting force to hold the substrates at a fixed separation, can then be calculated as the pressure imbalance, i.e. $\langle f_s \rangle = \langle P_{\perp} - P_b \rangle = \langle P_{\perp} \rangle - \langle P_{\parallel} \rangle$. In the limit of large surface separations where the confinement effects become insignificant, confined fluids will restore the pressure isotropy of normal fluids, i.e. $\langle P_{\perp} \rangle = \langle P_{\parallel} \rangle = P_b$, and the solvation force will vanish as required.

The state variables for each of the *NhPT* simulations individually are N, h, $P_{\parallel}$, and T. To investigate a confined fluid connected to the same reservoir at different h, a single set of $P_{\parallel}$ and T constraints should be used throughout. We set $T_b^* = 1.0(\varepsilon/k_B)$ and $P_{\parallel,\text{set}}^* = 0.49(\varepsilon/\sigma^3)$, equivalent to 120 K and 20.4 MPa if the LJ particles represent Ar atoms, for the purpose of comparing with existing results. In the light of the construction scheme of infinite substrates presented above, the same number of fluid atoms, namely 450 LJ particles, were used throughout the *NhPT* MD simulations regardless of h. This is a feature of important advantage over the previous *NAPT* method, particularly for simulations of large molecules and complex confined systems. The equations of motion were integrated using the fourth-order Gear predictor–corrector algorithm along with a dimensionless time step δt of 0.00232, corresponding to 5 fs for Ar. We began our simulations with the system having the widest h and smallest A. For a new h, a few hundred ps were used to achieve it. To assure equilibration before each production run, at least another 500 ps were spent and the time-averaged $P_{\perp}$, $P_{\parallel}$, density profile, and interaction energies were examined. Results reported here are based on production runs over 200,000 time steps, i.e. 1 ns for Ar. We have also tested a few cases by decreasing and increasing h and found the results to be reproducible.

RESULTS AND DISCUSSION

The uniqueness and success of the *NhPT* MD method lies mostly in the parallel-pressure control via instantaneous, differential adjustment of the transverse dimensions and coordinates. We therefore investigated the effectiveness of the pressure control first. For verification and demonstration, we show the test results from using a typical confined system in Fig. 2. It should be noted that, without the pressure control, our MD simulations are simplified to usual *NVT* simulations because both A and h will be fixed. Provided that the simulation system is equilibrated and the duration of simulation is sufficiently long, an *NVT* MD simulation could produce a mean pressure (cf. Fig. 2a). However, without such knowledge as an equation of state, this mean pressure either cannot be determined in advance or needs to be achieved by a painstaking process of trial and error. As demonstrated in Fig. 2a, the pressure control incorporated in the *NhPT* method can effectively bring the system to and maintain it at the target pressure with no need for an equation of state. In the meantime, the transverse dimension of the simulation box S_x, the conjugate variable to the parallel pressure, changes in accord with the pressure evolution and reaches a steady, equilibrium value as expected (cf. Fig. 2b). The speed of pressure and dimension evolution is governed by the coupling time constant t_p in the pressure control. A smaller t_p reaches the target pressure faster, but also could cause pressure overshoot (cf. Fig. 2b), which may be a disadvantage under some circumstances. Much too small a t_p may even cause the simulation to be unstable. On the other hand, as long as t_p is relatively large, it should cause only insignificant alterations to the structural and dynamical properties of an equilibrated system. We tested a few t_p in the range of 100–10,000 δt's, corresponding to 0.5–50 ps for Ar, which are all greater than the one used by Berendsen *et al.* [42,43] in their simulations of water. Nearly identical $P_{\parallel}$ and $P_{\perp}$ distributions, density profiles, and mean-square displacements were obtained. The pressure distributions, shown in Fig. 3, are all fitted well with Gaussian functions as would be expected of

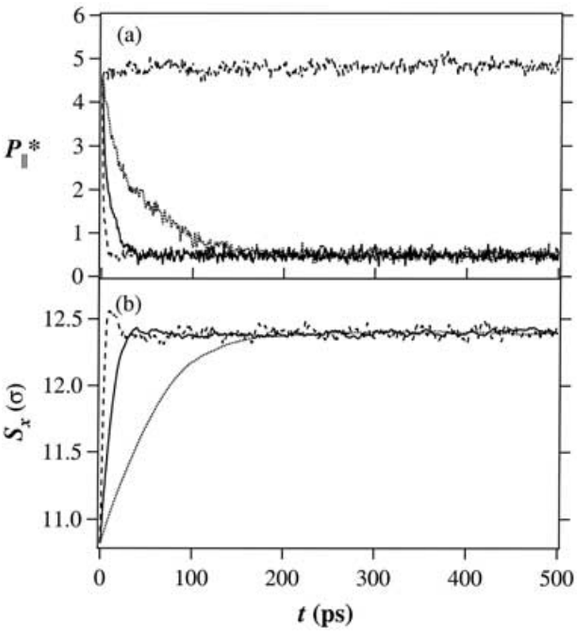

FIGURE 2 Time evolution of (a) reduced parallel pressure and (b) transverse dimension of the simulation box for the confined LJ fluid at $h = 4.6\sigma$ and $t_p = 100\,\delta t$'s (dashed curves), $500\,\delta t$'s (solid curves), and $2500\,\delta t$'s (dotted curves). Each point is averaged over $200\,\delta t$'s. The target pressure is 0.49. The horizontal dotted-dashed curve in (a) is the case without pressure control.

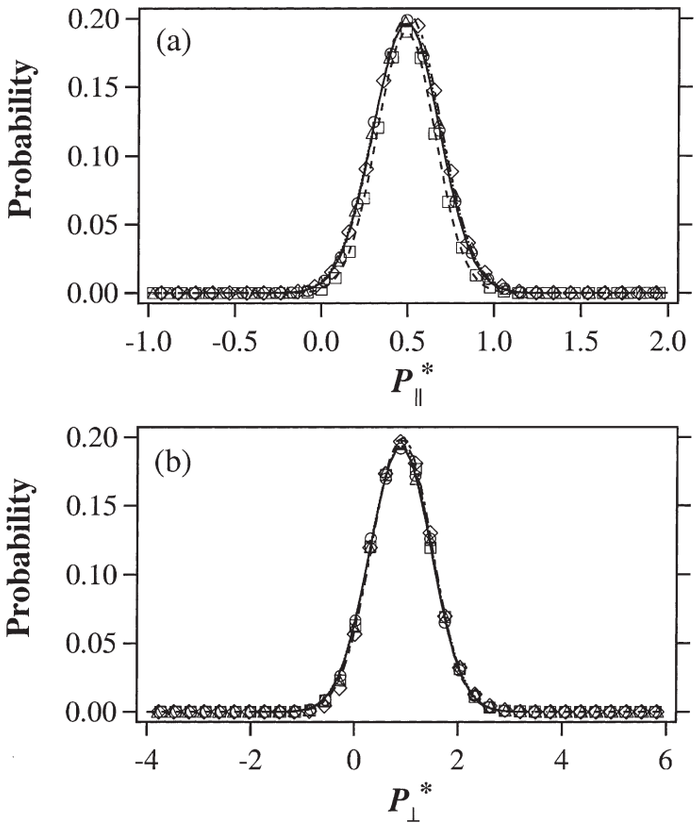

FIGURE 3 Probability distributions of (a) reduced parallel pressure and (b) reduced perpendicular pressure for the confined LJ film at $h = 4.6\sigma$ and $t_p = 100\,\delta t$'s (squares), $500\,\delta t$'s (circles), $2500\,\delta t$'s (triangles), and $10{,}000\,\delta t$'s (diamonds). Curves represent the best-fit Gaussian functions.

unaltered systems. It is thus believed that a t_p of 500 δt's adopted in our simulations is an appropriate value for the confined LJ fluid.

The results presented below are ensemble averages obtained in practice from time averages of corresponding instantaneous values. We drop $\langle\,\rangle$ from our discussions and figures for simplicity. Figure 4 displays the equilibrium transverse dimension as a function of surface separation together with the configuration snapshots at the largest and smallest surface separations. The *NhPT* MD simulation becomes unstable for confined films thinner than 2.1σ because fluid atoms form just one layer and rescaling their coordinates tends to cause them to run into substrate atoms. As h decreases, S_x naturally expands in order to comply with the pressure constraint with the same amount of fluid atoms. For comparison, the S_x vs. h relationship of a continuum, incompressible fluid is also attached as the dotted curve. It is obtained based on the conservation of the volume, $V = S_x^2(h - l/2)$ and l being the lattice constant, at $h = 8.5\sigma$. We used $(h - l/2)$ instead of h or $(h - \sigma)$ because it not only takes into account the actual volume accessible to the confined fluid but also recovers the molar volume/density of the fcc substrate when fluid atoms are perfectly ordered as substrate atoms. We found that, except when h is smaller than about 2.6σ, "negative" deviations of S_x from the incompressible, continuum behavior are observed, implying that simple fluid atoms can be packed more efficiently in confinement to occupy less volume than in thicker films or bulk reservoir. More importantly, step-like changes indicative of sudden expansion/contraction of S_x take place and become more pronounced at smaller separations. Apparently, the negative deviations are resulted from the formation of fluid layers and the step-like changes are caused by sudden decrease/increase in the number of fluid layers. In general, confined films between two consecutive "convex" corners, e.g. $h = 4.1\sigma$ and 3.0σ, have the same number of fluid layers. A quasi-constant S_x over a range of h suggests marked density changes and hence structural transitions between ordered and disordered states. These fluid layers, density changes, and structural transitions can be readily portrayed with density profiles. For this purpose, we show representative density profiles within the tri-layer regime in Fig. 5. Clearly, upon increasing or decreasing h, average density and degree of layering of the confined fluid

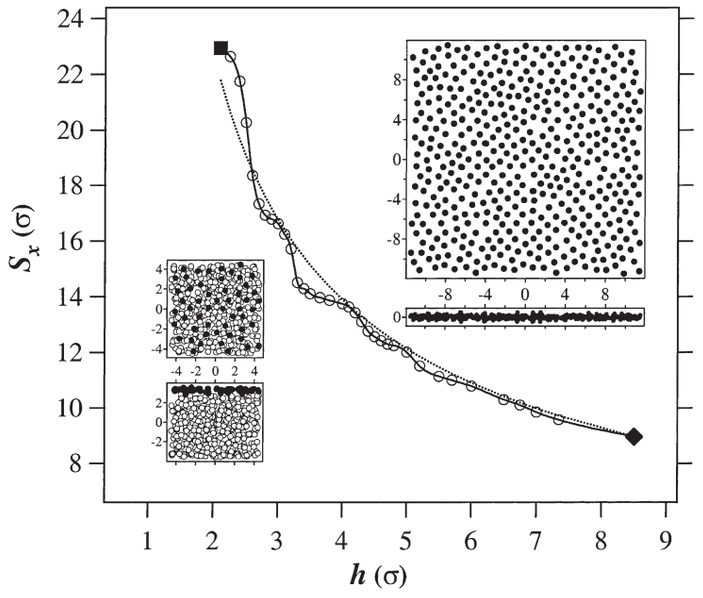

FIGURE 4 Equilibrium transverse dimension of the simulation box as a function of surface separation. Dotted curve indicates the behavior of a continuum, incompressible fluid. Also shown are the top-down (xy) and side (xz) views of the confined LJ films at $h = 8.5\sigma$ (left insets) and 2.1σ (right insets), where solid circles represent the fluid atoms in the contact layer adjacent to the top confining surface and open circles represent the rest of fluid atoms.

change in response, even though the number of fluid layers remains the same. Confined films at convex corners in Fig. 4 can be understood to have locally minimum densities and minimum negative deviations. Interestingly, these minimum densities are very close to those of thicker films and very likely the corresponding bulk density too. They also correlate well with minimum degrees of layering as shown in Fig. 5. Contrarily, as S_x reaches "concave" corners, e.g. $h = 3.3\sigma$, locally maximum densities, maximum negative deviations, and maximum degrees of layering occur. A slight decrease in h is then enough to force the fluid atoms to undergo sudden expansion in the transverse directions at the cost of a one-layer reduction in the number of fluid layers.

Traditional simulation studies of confined fluids have used simulation boxes of fixed surface areas. One of the important results common to these studies is the dependence of the number of confined molecules N on surface separation h. For the *NhPT* method to make connection and comparison, simulation data were converted to surface density (N/A) vs. h and are plotted in Fig. 6. The resultant step-like relationship is in excellent agreement with that from the *NAPT* study [38] and with others reported previously [10,17,45]. Note that the concave

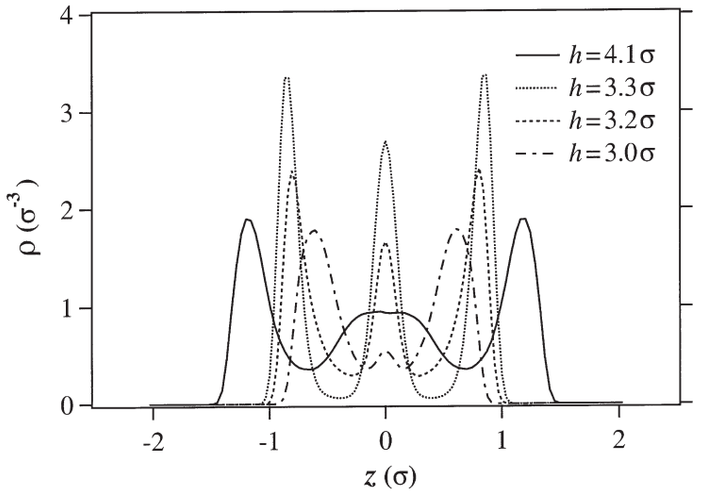

FIGURE 5 Equilibrium density profiles of representative confined films within the trilayer regime.

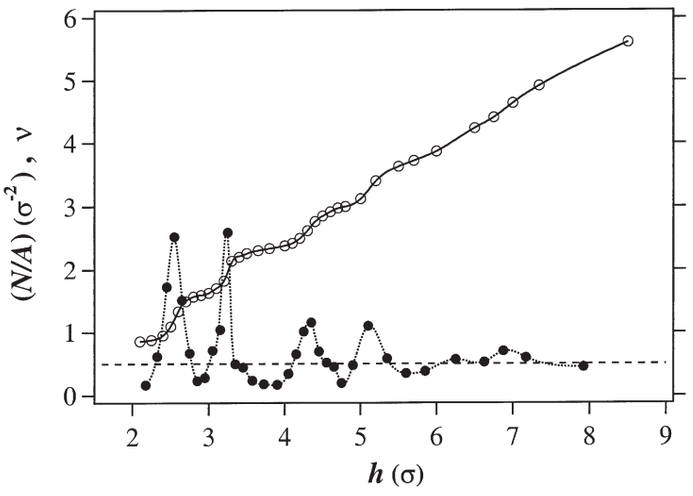

FIGURE 6 Surface density (N/A) (open circles) and pseudo-Poisson's ratio ν (solid circles) of the confined LJ fluid as a function of surface separation. The dashed line indicates $\nu = 0.5$.

corners in S_x vs. h (cf. Fig. 4) become the convex ones in (N/A) vs. h (cf. Fig. 6) and vice versa. In other words, maximum density and degree of layering occur at the top of each step riser in (N/A) vs. h, while minimum ones occur at the bottom. Also indicated in Fig. 4 and in the literature [3,5–9,11–13,32] is that confined fluids can have densities and degrees of ordering not only significantly higher than those of liquids but also close to solids. Consequently, they have been quite often referred to as solid-like matter. It would then be interesting to extend the characterization methods of solids to confined fluids. When a solid is in longitude strain, it tends to change its dimensions in the directions perpendicular to the applied stress. The dimensionless ratio of the relative length changes along the parallel and perpendicular directions is called the Poisson ratio [46]. We have attempted the calculation of a pseudo-Poisson's ratio for confined simple fluid using the following definition,

$$\nu = -\frac{(\Delta S_x/S_x)}{(\Delta h/h)}. \tag{16}$$

The results, shown in Fig. 6, are very unlike typical solids whose values are usually fixed and between 0.3 and 0.5 [46]. The Poisson ratio, as high as 2.6 and as low as 0.17, oscillates with surface separation and coincides with step changes. Not surprisingly, it rises to maxima during the sudden expansion/contraction of S_x and drops to minima when S_x is virtually constant and films are disordered. Interestingly, when the separation becomes sufficiently large, the Poisson ratio appears to converge to the limiting value of 0.5, which is for incompressible continua and indicative of the conservation of volume $V = S_x^2(h - l/2)$.

Perpendicular pressure $P_\perp$, or equivalently negative normal stress, is perhaps the most looked at property of confined fluids because of its direct connection to SFA experiments and its important relevance to many technological fields. The average perpendicular pressures from the *NhPT* MD simulations are shown in Fig. 7. Consistent with previous simulation studies [12,17,35,36,38,39,41,45], it oscillates with surface separation, with maximum occurring in the best-layered films and minima in disordered films, and approaches the set parallel (bulk) pressure when the surface separation becomes sufficiently large. More importantly, it agrees quantitatively well with the previous GCMC studies [45,47] of confined simple fluids subject to the same bulk temperature and pressure, except the height of the secondary peak around $h = 3.3\sigma$. Given the considerable differences in the employed ensembles and simulations techniques, such an agreement is of remarkable significance and strengthens the credibility of the *NhPT* method for studying confined fluids.

It has been known that confinement induces not only layering in the perpendicular direction but also ordering in the transverse directions [11,12,41]. Such transverse in-plane ordering, as revealed by the insets in Fig. 4, should resemble the atomic structure of the confining surfaces. To quantify the degrees of in-plane ordering for the many surface separations considered in this work, we opted for a relatively simple measure and adopted the following structure factor [32],

$$S_k = \left| \frac{1}{N} \sum_{i=1}^{N} e^{i\mathbf{k}^\lambda \cdot \mathbf{r}_i^\lambda} \right|^2, \tag{17}$$

where $\mathbf{r}_i^\lambda$ is the transverse coordinate of atom i and $\mathbf{k}^\lambda$ is a two-dimensional reciprocal lattice vector

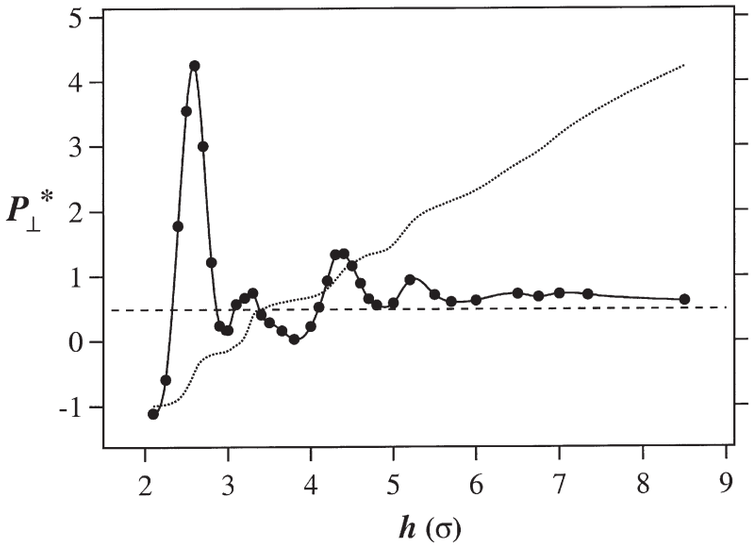

FIGURE 7 Reduced perpendicular pressure as a function of surface separation. The dashed line denotes $P^*_{\parallel,\mathrm{set}} = 0.49$ and the dotted curve is scaled surface-density profile.

pertinent to the fcc(100) confining surfaces. To characterize a single fcc(100) layer, one of the shortest $\mathbf{k}^\lambda$ based on our coordinate system, $\mathbf{k}_1 = (2\pi/l)(1,1)$ and l being the lattice constant, is suitable. The limiting values of S_{k1}, the structural factor calculated using $\mathbf{k}_1$, are 1 for a layer of fluid atoms in perfect fcc(100) lattice and 0 for bulk liquids. However, for a fcc(100) slab with repeating $\ldots abab\ldots$ layers, where b is structurally identical to a but displaced by $0.5l$ in the x or y direction, contributions to S_{k1} from successive ab layers cancel each other out. For this reason, S_{k1} becomes insensitive to in-plane ordering transitions in confined films having three fluid layers or more (cf. Fig. 8). To clarify them, we used a larger reciprocal lattice vector $\mathbf{k}_2 = (4\pi/l)(1,1)$ to calculate S_{k2}. For a perfect fcc(100) layer and normal liquids, S_{k2} has the same limiting values as S_{k1}. However, as can be seen in Fig. 8, S_{k2} is more sensitive for confined films with more than two layers. It is particularly so for the films forming three well-ordered fluid layers (cf. $h = 3.3\sigma$ in Figs. 5 and 8), which tend to be of the commensurate aba structure between the in-registry confining surfaces. On the other hand, the bi-layer thinner films are incommensurate with the employed confining surfaces, so that their transverse structures are distorted with plenty of structural irregularities

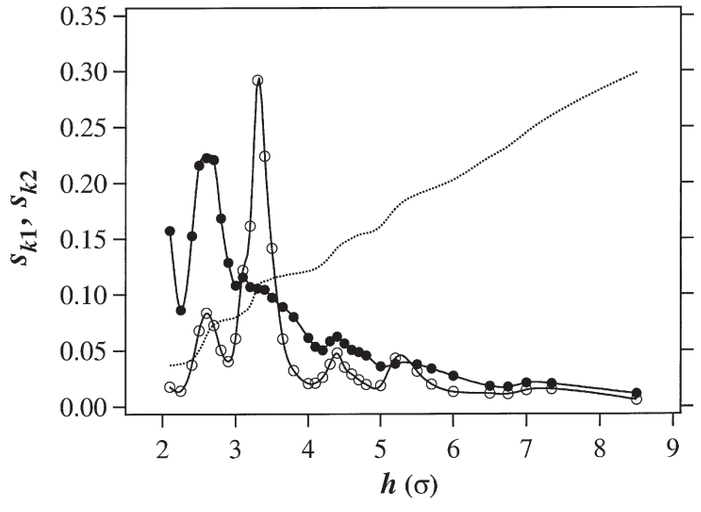

FIGURE 8 Structural factors as a function of surface separation. Solid and open circles represent S_{k1} and S_{k2}, respectively (see text). The dotted curve is scaled surface-density profile.

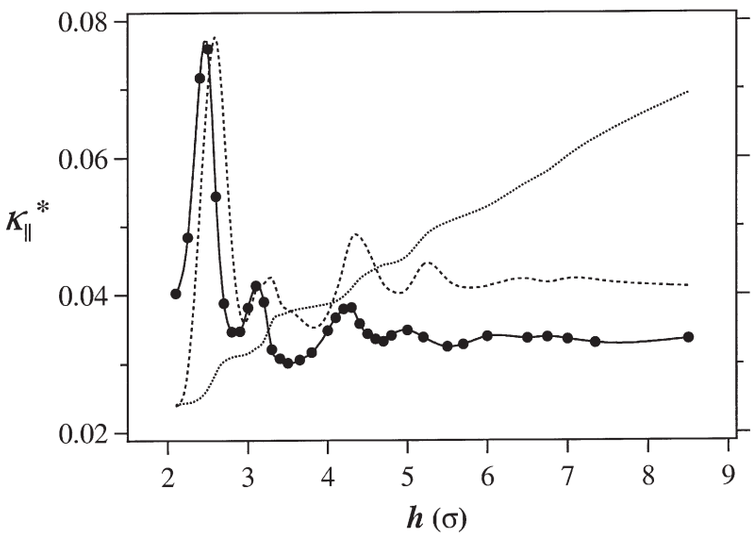

FIGURE 9 Transverse isothermal compressibility as a function of surface separation. The dotted curve is scaled surface-density profile and the dashed curve is scaled perpendicular-pressure profile.

and voids. This leads to their lower S_{k2}. When compared, S_{k2} correlates very well with the perpendicular pressure, both rising to maximum values when confined films are best layered and drop to minimum values when films become disordered. In other words, the transverse in-plane ordering in the confined simple fluid synchronizes with layering in the perpendicular direction. Fluid atoms must order themselves to the highest degree in the transverse directions in order to achieve a maximum degree of layering.

The parallel-pressure control that we derived for the *NhPT* MD simulations of confined simple fluids contains a transverse isothermal compressibility $\kappa_\parallel$, whose microscopic expression is given in Eqs. (13) and (A.16) in Appendix I. Instantaneous $\kappa_\parallel$ was calculated during our simulations and the averaged values are shown in Fig. 9. Like other properties of confined fluids, $\kappa_\parallel$ oscillates at small separations and stabilizes at large separations to a specific value, $0.033\sigma^3/\varepsilon$ under the specified T and $P_{\parallel,\text{set}}$ in this work. This limiting value as well as those oscillatory $\kappa_\parallel$ are found to be fittingly between and of the same order of magnitude as $0.017\sigma^3/\varepsilon$ for an amorphous LJ solid [48] and $0.11\sigma^3/\varepsilon$ for a LJ liquid [49] under a similar condition. Previous MC studies [41,50] have also estimated $\kappa_\parallel$ for confined simple fluids in the bi- and tri-layer regimes through a Gibbs–Duhem relation and fluctuations in the number of fluid atoms. Thermodynamic condition and model detail were found to have a significant impact on the magnitude of $\kappa_\parallel$ [41,50] which, in conjunction with calculation approach, may explain the difference between the results presented here and in the previous studies. One important finding in common though is that $\kappa_\parallel$, as illustrated in Fig. 9, does not correlate exactly with the perpendicular pressure. Instead, its peak values shift towards the concave corners in the surface-density profiles where the confined films are least dense, least ordered, and consequently most compressible. The bi-layer films are exceptionally compressible, which can be attributed to their incommensurateness, that causes structural voids and positive S_x deviations.

As mentioned earlier, the *NhPT* MD method possesses a desirable advantage over other methods for its ability to systematically probe the dynamical properties of confined fluids. The dynamical properties can be expected to depend on the surface separation, like the structural properties discussed above, and furthermore differ along the perpendicular and transverse directions due to the confined environment and anisotropic configurations. In this respect, we investigate here the diffusivity parallel to the confining substrates through the following Einstein relation [42],

$$D_\parallel = \lim_{t\to\infty} \frac{\langle [r_\parallel(t) - r_\parallel(0)]^2 \rangle}{4t}, \tag{18}$$

where $\langle [r_\parallel(t) - r_\parallel(0)]^2 \rangle$ is the ensemble-averaged mean-square displacement in the transverse directions. The results are displayed in Fig. 10, where the attached inset shows the mean-square displacement corresponding to the smallest $D_\parallel$ obtained in this work. The linearity of the displacement curve clearly indicates that the time scale used, corresponding to 512 ps if the LJ particles are Ar atoms, is long enough for every confined film to enter the diffusive regime. Although not calculated, the diffusivities in the perpendicular direction are practically zero over the same time scale since the displacement of fluid atoms is impeded by the layered configurations and

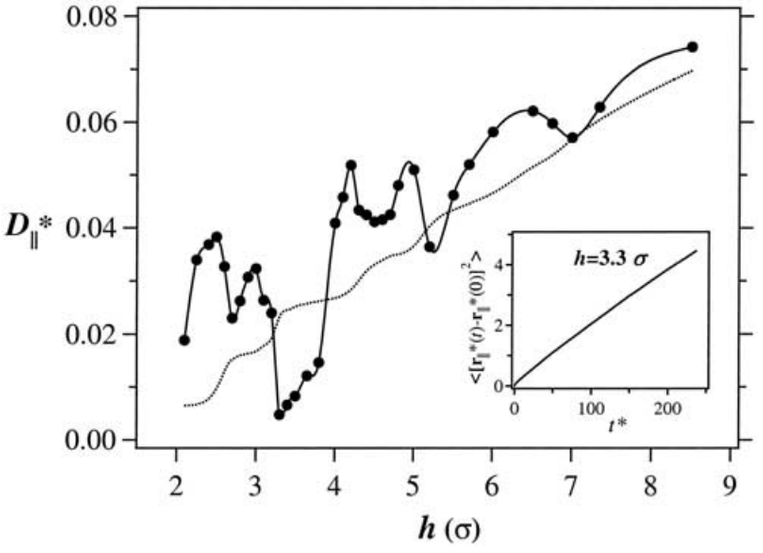

FIGURE 10 Transverse diffusivity as a function of surface separation. The dotted curve is scaled surface-density profile. The inset is the ensemble-averaged mean-square displacement in the transverse directions at $h = 3.3\sigma$.

restricted by the confining substrates [16]. In Fig. 10, $D_{\|}$ can be seen clearly to exhibit oscillations of the same periodicities as those properties discussed above. Based on the connections between the surface separation, density, and degree of ordering, we can conclude that confined films having ordered configurations and high densities give rise to minimum diffusivities, while those films having disordered configurations and low densities result in maximum diffusivities. Similar correlations have also been reported in previous MD simulations [14,16,17,23,38]. Here we want to note that even the best ordered film at $h = 3.3\sigma$ is not very solid-like because its transverse diffusivity, very detectable despite being the lowest, suggests that fluid atoms still remain quite mobile. In additional, by examining the incompressible curve in Fig. 4 and the $D_{\|}$ in Fig. 10, it is revealed that density alone is not sufficient to explain all the features of the diffusivity. We need to factor in the fraction of fluid atoms in the contact layers, whose diffusivities are more reduced that those in the middle [14] portion of the confined space. As surface separation widens, this fraction decreases, and $D_{\|}$ generally increases and approaches the bulk diffusivity.

SUMMARY

We have successfully developed an *NhPT* MD method for the purpose of systematically investigating the structural and dynamical properties of confined fluids. In this method, temperature and parallel-pressure constraints are employed as virtual reservoir to subject confined fluids to the same equilibrium condition regardless of surface separation. The parallel pressure is intended to be controlled by instantaneous, differential scaling of the transverse dimensions of simulations box and the transverse coordinates of fluid molecules accordingly. However, such scaling and periodic boundary conditions are applied only to the confined fluids in order not to alter the crystalline structure of the confining substrates. To achieve pressure control computationally for the *NhPT* method, Berendsen's loose coupling method was found to be adequate and hence adopted. In addition, a microscopic expression of transverse isothermal compressibility is obtained as a by-product of the derivation. As the separation varies between confining substrates, the *NhPT* MD method allows the simulation system to expand or contract transversely so that the same number of confined molecules can be simulated. This is an important, desirable advantage over other methods, especially for confined large, complex molecules such as polymers and biomolecules.

We first implemented the *NhPT* MD method using a confined LJ fluid. As reported previously, confinement induces fluid atoms to form not only layers stacking in the perpendicular direction but also transversely ordered configurations reflecting the atomic structure of the substrates. As the surface separation varies, step-like changes occur in the transverse dimension of the simulation box, of which a quasi-constant value indicates no change in the number of fluid layers but marked changes in the pore density and structural orderings, and a sharp expansion/contraction signals a sudden change in the number of fluid layers. With this relationship, a pseudo-Poisson's ratio was calculated for the confined fluid and found to oscillate with surface separation. It rises to a maximum during a sudden

expansion/contraction of the transverse dimension and drops to a minimum when the transverse dimension is virtually constant. More interestingly, it approaches a limiting value corresponding to the Poisson ratio for incompressible continua when the surface separation is sufficiently large. Analyses of density profiles and structural factors revealed that maxima in the degree of layering are accompanied by maxima in the pore density and degree of in-plane ordering. Consistent with previous studies, such maxima also give rise to maximum perpendicular pressures and minimum transverse diffusivities. When confined films become disordered and possess bulk-like densities, minimum perpendicular pressures and maximum diffusivities take place. Transverse isothermal compressibility, like other properties, also oscillates at small separations and stabilizes at large separations to a specific value. However, it does not correlate exactly with the pore density or perpendicular pressure. Instead its peak values occur towards where the confined films are least dense, least ordered, and consequently most compressible.

Acknowledgements

We are grateful to the Missouri Research Board for partial support of this research.

APPENDIX I

Dilation Coefficient χ for the *NhPT* MD Method

The xx component of the pressure tensor for a simple confined fluid can be expressed as,

$$P_{xx}S_xS_yh = \sum_i \left(\mathbf{p}_i^x \cdot \mathbf{p}_i^x\right)/m_i + \frac{1}{2}\sum_i \sum_{j\neq i} \mathbf{f}_{\mathrm{ij}}^x \cdot \mathbf{r}_{ij}^x + \sum_i \sum_s \mathbf{f}_{is}^x \cdot r_{is}^x. \tag{A.1}$$

Its partial differentiation with respect to S_x under a constant temperature yields

$$\frac{\partial P_{xx}}{\partial S_x} S_xS_yh + P_{xx}S_yh = \frac{1}{2}\sum_i \sum_{j\neq i} \left(\frac{\partial \mathbf{f}_{ij}^x}{\partial S_x}\cdot \mathbf{r}_{ij}^x + \mathbf{f}_{ij}^x \cdot \frac{\partial \mathbf{r}_{ij}^x}{\partial S_x}\right) + \sum_i \sum_s \left(\frac{\partial \mathbf{f}_{is}^x}{\partial S_x}\cdot \mathbf{r}_{is}^x + \mathbf{f}_{is}^x \cdot \frac{\partial \mathbf{r}_{is}^x}{\partial S_x}\right). \tag{A.2}$$

To adjust P_{xx} instantaneously, we scale the transverse dimensions of simulation box based on $(\delta S_\lambda/\delta t) = \chi S_\lambda$, and the transverse coordinates of fluid atoms based on $(\delta \mathbf{r}_{ij}^\lambda/\delta t) = \chi \mathbf{r}_{ij}^\lambda$. This is a uniform scaling scheme in accord with the equation of motion, Eq. (4). In consequence,

$$\frac{\partial \mathbf{r}_{ij}^\lambda}{\partial S_\lambda} = \frac{\delta \mathbf{r}_{ij}^\lambda}{\delta S_\lambda} = \frac{\mathbf{r}_{ij}^\lambda}{S_\lambda}, \tag{A.3}$$

$$\frac{\partial r_{ij}}{\partial S_\lambda} = \frac{\mathbf{r}_{ij}^\lambda}{r_{ij}} \cdot \frac{\mathbf{r}_{ij}^\lambda}{S_\lambda}. \tag{A.4}$$

With the chain rule and Eqs. (A.3) and (A.4), we can get for the fluid–fluid interactions,

$$\frac{\partial \mathbf{f}_{ij}^x}{\partial S_x} = \frac{\partial}{\partial S_x}\left(-\frac{\mathrm{d}U}{\mathrm{d}r}\frac{\mathbf{r}_{ij}^x}{r_{ij}}\right) = \frac{\mathbf{r}_{ij}^x}{r_{ij}^4 S_x}\left[\left(-r_{ij}^2\frac{\mathrm{d}^2U}{\mathrm{d}r^2} + r_{ij}\frac{\mathrm{d}U}{\mathrm{d}r}\right)\left(\mathbf{r}_{ij}^x \cdot \mathbf{r}_{ij}^x\right) - r_{ij}^3\frac{\mathrm{d}U}{\mathrm{d}r}\right], \tag{A.5}$$

and

$$\frac{\partial \mathbf{f}_{ij}^x}{\partial S_x}\cdot \mathbf{r}_{ij}^x + \mathbf{f}_{ij}^x \cdot \frac{\partial \mathbf{r}_{ij}^x}{\partial S_x} = \frac{1}{r_{ij}^4 S_x}\left[\left(-r_{ij}^2\frac{\mathrm{d}^2U}{\mathrm{d}r^2} + r_{ij}\frac{\mathrm{d}U}{\mathrm{d}r}\right)\left(\mathbf{r}_{ij}^x \cdot \mathbf{r}_{ij}^x\right) - 2r_{ij}^3\frac{\mathrm{d}U}{\mathrm{d}r}\right]. \tag{A.6}$$

For the fluid–substrate interactions, we scale via $(\delta \mathbf{r}_{is}^\lambda/\delta t) = \chi \mathbf{r}_i^\lambda$ because substrate atoms should be stationary to keep the atomic structure of the substrates intact. Consequently,

$$\frac{\partial \mathbf{f}_{is}^x}{\partial S_x}\cdot \mathbf{r}_{is}^x + \mathbf{f}_{is}^x \cdot \frac{\partial \mathbf{r}_{is}^x}{\partial S_x} = \frac{1}{r_{is}^4 S_x}\left[\left(-r_{is}^2\frac{\mathrm{d}^2U}{\mathrm{d}r^2} + r_{is}\frac{\mathrm{d}U}{\mathrm{d}r}\right)\left(\mathbf{r}_{is}^x \cdot \mathbf{r}_{is}^x\right) - 2r_{is}^3\frac{\mathrm{d}U}{\mathrm{d}r}\right]. \tag{A.7}$$

Now Eq. (A.2) can be rearranged to give

$$\frac{1}{\kappa_{xx}} = -\frac{\partial P_{xx}}{\partial S_x}S_x = P_{xx} - \frac{1}{S_xS_yh}\left\{\frac{1}{2}\sum_i \sum_{j\neq i}\left[\frac{X(r_{ij})}{r_{ij}^4}\left(\mathbf{r}_{ij}^x \cdot \mathbf{r}_{ij}^x\right) - \frac{2}{r_{ij}}\frac{\mathrm{d}U}{\mathrm{d}r}\right]\left(\mathbf{r}_{ij}^x \cdot \mathbf{r}_{ij}^x\right) + \sum_i \sum_s \left[\frac{X(r_{is})}{r_{is}^4}\left(\mathbf{r}_{is}^x \cdot \mathbf{r}_{is}^x\right) - \frac{2}{r_{is}}\frac{\mathrm{d}U}{\mathrm{d}r}\right]\left(\mathbf{r}_{is}^x \cdot \mathbf{r}_i^x\right)\right\}, \tag{A.8}$$

where

$$X(r) = -r^2\frac{\mathrm{d}^2U}{\mathrm{d}r^2} + r\frac{\mathrm{d}U}{\mathrm{d}r}. \tag{A.9}$$

The partial differentiation of Eq. (A.1) with respect to S_y yields

$$\frac{\partial P_{xx}}{\partial S_y} S_x S_y h + P_{xx} S_x h = \frac{1}{2} \sum_i \sum_{j \neq 1} \left(\frac{\partial \mathbf{f}_{ij}^x}{\partial S_y} \cdot \mathbf{r}_{ij}^x \right) + \sum_i \sum_s \left(\frac{\partial \mathbf{f}_{is}^x}{\partial S_y} \cdot r_{is}^x \right). \quad \text{(A.10)}$$

Again, for the fluid–fluid and fluid–substrate interactions, we can drive the following expressions,

$$\frac{\partial \mathbf{f}_{ij}^x}{\partial S_y} = \frac{\partial}{\partial S_y} \left(-\frac{\mathrm{d}U}{\mathrm{d}r} \frac{\mathbf{r}_{ij}^x}{r_{ij}} \right) = \frac{\mathbf{r}_{ij}^x}{r_{ij}^4 S_y} \left[\left(-r_{ij}^2 \frac{\mathrm{d}^2 U}{\mathrm{d}r^2} + r_{ij} \frac{\mathrm{d}U}{\mathrm{d}r} \right) \left(\mathbf{r}_{ij}^y \cdot \mathbf{r}_{ij}^y \right) \right], \quad \text{(A.11)}$$

$$\frac{\partial \mathbf{f}_{is}^x}{\partial S_y} = \frac{\partial}{\partial S_y} \left(-\frac{\mathrm{d}U}{\mathrm{d}r} \frac{\mathbf{r}_{is}^x}{r_{is}} \right) = \frac{\mathbf{r}_{is}^x}{r_{is}^4 S_y} \left[\left(-r_{is}^2 \frac{\mathrm{d}^2 U}{\mathrm{d}r^2} + r_{is} \frac{\mathrm{d}U}{\mathrm{d}r} \right) \left(\mathbf{r}_{is}^y \cdot \mathbf{r}_i^y \right) \right]. \quad \text{(A.12)}$$

As a result,

$$\frac{1}{\kappa_{yx}} = -\frac{\partial P_{xx}}{\partial S_y} S_y = P_{xx} - \frac{1}{S_x S_y h} \left\{ \frac{1}{2} \sum_i \sum_{j \neq i} \left[\frac{X(r_{ij})}{r_{ij}^4} \left(\mathbf{r}_{ij}^y \cdot \mathbf{r}_{ij}^x \right) \right] \left(\mathbf{r}_{ij}^y \cdot \mathbf{r}_{ij}^y \right) + \sum_i \sum_s \left[\frac{X(r_{is})}{r_{is}^4} \left(\mathbf{r}_{is}^x \cdot \mathbf{r}_{is}^x \right) \right] \left(\mathbf{r}_{is}^y \cdot \mathbf{r}_i^y \right) \right\}. \quad \text{(A.13)}$$

Similarly, using the *yy* component of the pressure tensor yields

$$\frac{1}{\kappa_{yy}} = -\frac{\partial P_{yy}}{\partial S_y} S_y = P_{yy} - \frac{1}{S_x S_y h} \left\{ \frac{1}{2} \sum_i \sum_{j \neq i} \left[\frac{X(r_{ij})}{r_{ij}^4} \left(\mathbf{r}_{ij}^y \cdot \mathbf{r}_{ij}^y \right) - \frac{2}{r_{ij}} \frac{\mathrm{d}U}{\mathrm{d}r} \right] \left(\mathbf{r}_{ij}^y \cdot \mathbf{r}_{ij}^y \right) + \sum_i \sum_s \left[\frac{X(r_{is})}{r_{is}^4} \left(\mathbf{r}_{is}^y \cdot \mathbf{r}_{is}^y \right) - \frac{2}{r_{is}} \frac{\mathrm{d}U}{\mathrm{d}r} \right] \left(\mathbf{r}_{is}^y \cdot \mathbf{r}_i^y \right) \right\}, \quad \text{(A.14)}$$

$$\frac{1}{\kappa_{xy}} = -\frac{\partial P_{yy}}{\partial S_x} S_x = P_{yy} - \frac{1}{S_x S_y h} \left\{ \frac{1}{2} \sum_i \sum_{j \neq i} \left[\frac{X(r_{ij})}{r_{ij}^4} \left(\mathbf{r}_{ij}^y \cdot \mathbf{r}_{ij}^y \right) \right] \left(\mathbf{r}_{ij}^x \cdot \mathbf{r}_{ij}^x \right) + \sum_i \sum_s \left[\frac{X(r_{is})}{r_{is}^4} \left(\mathbf{r}_{is}^y \cdot \mathbf{r}_{is}^y \right) \right] \left(\mathbf{r}_{is}^x \cdot \mathbf{r}_i^x \right) \right\}. \quad \text{(A.15)}$$

Combining Eqs. (A.8), (A.13), (A.14) and (A.15) leads to

$$\frac{1}{\kappa_{\|}} = \frac{\left(P_{xx} + P_{yy} \right)}{2} - \frac{1}{4 S_x S_y h} \left\{ \frac{1}{2} \sum_i \sum_{j \neq i} \left[\frac{X(r_{ij})}{r_{ij}^4} \left(\mathbf{r}_{ij}^\lambda \cdot \mathbf{r}_{ij}^\lambda \right) - \frac{2}{r_{ij}} \frac{\mathrm{d}U}{\mathrm{d}r} \right] \left(\mathbf{r}_{ij}^\lambda \cdot \mathbf{r}_{ij}^\lambda \right) + \sum_i \sum_s \left[\frac{X(r_{is})}{r_{is}^4} \left(\mathbf{r}_{is}^\lambda \cdot \mathbf{r}_{is}^\lambda \right) - \frac{2}{r_{is}} \frac{\mathrm{d}U}{\mathrm{d}r} \right] \left(\mathbf{r}_{is}^\lambda \cdot \mathbf{r}_i^\lambda \right) \right\}, \quad \text{(A.16)}$$

where, for convenience, we have used the notation: $\mathbf{r}^\lambda \cdot \mathbf{r}^\lambda = \mathbf{r}^x \cdot \mathbf{r}^x + \mathbf{r}^x \cdot \mathbf{r}^x$.

References

[1] Horn, R.G. and Israelachvili, J.N. (1981) "Direct measurement of structural forces between two surfaces in a nonpolar liquid", *J. Chem. Phys.* **75**, 1400.

[2] Christenson, H.K. (1983) "Experimental measurements of solvation forces in nonpolar liquids", *J. Chem. Phys.* **78**, 6906.

[3] Gee, M.L., McGuiggan, P.M., Israelachvili, J.N. and Homola, A.M. (1990) "Liquid to solidlike transitions of molecularly thin films under shear", *J. Chem. Phys.* **93**, 1895.

[4] Gee, M.L. and Israelachvili, J.N. (1990) "Interactions of surfactant monolayers across hydrocarbon liquids", *J. Chem. Soc. Faraday Trans.* **86**, 4049.

[5] Israelachvili, J.N., McGuiggan, P.M. and Homola, A.M. (1988) "Dynamic properties of molecularly thin liquid films", *Science* **240**, 189.

[6] Granick, S., Demirel, A.L., Cai, L.L. and Peanasky, J. (1995) "Soft matter in a tight spot: nanorheology of confined liquids and block copolymers", *Isr. J. Chem.* **35**, 75.

[7] Demirel, A.L. and Granick, S. (1996) "Glasslike transition of a confined simple fluid", *Phys. Rev. Lett.* **77**, 2261.

[8] Klein, J. and Kumacheva, E. (1998) "Simple liquids confined to molecularly thin layers. I. Confinement-induced liquid-to-solid phase transitions", *J. Chem. Phys.* **108**, 6996.

[9] Kumacheva, E. and Klein, J. (1998) "Simple liquids confined to molecularly thin layers. II. Shear and frictional behavior of solidified films", *J. Chem. Phys.* **108**, 7010.

[10] Snook, I.K. and van Megan, W. (1980) "Solvation forces in simple dense fluids. I", *J. Chem. Phys.* **72**, 2907.

[11] Rhykerd, Jr., C.L., Schoen, M. and Diestler, D.J. (1987) "Epitaxy in simple classical fluids in micropores and new-solid surfaces", *Nature* **330**, 461.

[12] Schoen, M., Diestler, D.J. and Cushman, J.H. (1987) "Fluids in micropores. I. Structure of a simple classical fluid in a slit-pore", *J. Chem. Phys.* **87**, 5464.

[13] Miyahara, M. and Gubbins, K.E. (1997) "Freezing/melting phenomena for Lennard–Jones methane in slit pores: a Monte Carlo study", *J. Chem. Phys.* **106**, 2865.

[14] Somers, S.A. and Davis, H.T. (1992) "Microscopic dynamics of fluids confined between smooth and atomically structured solid surfaces", *J. Chem. Phys.* **96**, 5389.

[15] Toxvaerd, S. (1981) "The structure and thermodynamics of a solid-fluid interface", *J. Chem. Phys.* **74**, 1998.

[16] Magda, J.J., Tirrell, M. and Davis, H.T. (1985) "Molecular dynamics of narrow, liquid-filled pores,", *J. Chem. Phys.* **83**, 1888.

[17] Gao, J., Luedtke, W.D. and Landman, U. (1997) "Layering transitions and dynamics of confined liquid films", *Phys. Rev. Lett.* **79**, 705.

[18] Vanderlick, T.K., Scriven, L.E. and Davis, H.T. (1989) "Molecular theories of confined fluids", *J. Chem. Phys.* **90**, 2422.

[19] Lastoskie, C., Gubbins, K.E. and Quirke, N. (1993) "Pore size heterogeneity and the carbon slit pore: a density functional theory model", *Langmuir* **9**, 2693.
[20] Sarman, S. (1990) "The influence of the fluid-wall interaction potential on the structure of a simple fluid in a narrow slit", *J. Chem. Phys.* **92**, 4447.
[21] Duda, Y., Henderson, D., Trokhymchuk, A. and Wasan, D. (1999) "Integral equation study of the solvation force between macroscopic surfaces separated by thin films of diatomic chain, and network solvents", *J. Phys. Chem. B* **103**, 7495.
[22] Davis, H.T. (1987) "Kinetic theory of inhomogeneous fluid: tracer diffusion", *J. Chem. Phys.* **86**, 1474.
[23] Vanderlick, T.K. and Davis, H.T. (1987) "Self-diffusion in fluids in microporous solids", *J. Chem. Phys.* **87**, 1791.
[24] Pozhar, L.A. and Gubbins, K.E. (1991) "Dense inhomogeneous fluids: functional perturbation theory, the generalized Langevin equation, and kinetic theory", *J. Chem. Phys.* **94**, 1367.
[25] Pozhar, L.A. and Gubbins, K.E. (1993) "Transport theory of dense, strongly inhomogeneous fluids", *J. Chem. Phys.* **99**, 8970.
[26] Pozhar, L.A. (2000) "Structure and dynamics of nanofluids: theory and simulations to calculate viscosity", *Phys. Rev. E* **61**, 1432.
[27] Powles, J.G., Evans, W.A.B. and Quirke, N. (1982) "Non-destructive molecular-dynamics simulation of the chemical potential of a fluid", *Mol. Phys.* **46**, 1347.
[28] Gupta, S., Koopman, D.C., Westermann-Clark, G.B. and Bitsanis, I.A. (1994) "Segmental dynamics and relaxation of *n*-octane at solid-liquid interfaces", *J. Chem. Phys.* **100**, 8444.
[29] Winkler, R.G., Gerstmair, A., Reineker, P., Matsuda, T. and Yoon, D.Y. (1994) "Molecular dynamics simulations of *n*-alkane melts confined between solid surfaces", *Int. J. Quan. Chem.* **52**, 437.
[30] Clifton, B. and Cosgrove, T. (1998) "Simulation of liquid benzene between two graphite surfaces: a molecular dynamics study", *Mol. Phys.* **93**, 767.
[31] Padilla, P. and Toxvaerd, S. (1994) "Fluid alkanes in confined geometries", *J. Chem. Phys.* **101**, 1490.
[32] Thompson, P.A., Robbins, M.O. and Grest, G.S. (1995) "Structure and shear response in nanometer-thick films", *Isr. J. Chem.* **35**, 93.
[33] Ballamudi, R.K. and Bitsanis, I.A. (1996) "Energetically driven liquid–solid transitions in molecularly thin *n*-octane films", *J. Chem. Phys.* **105**, 7774.
[34] Stevens, M.J., Mondello, M., Grest, G.S., Cui, S.T., Cochran, H.D. and Cummings, P.T. (1997) "Comparison of shear flow of hexadecane in a confined geometry and in bulk", *J. Chem. Phys.* **106**, 7303.
[35] Wang, Y., Hill, K. and Harris, J.G. (1994) "Confined thin films of a linear and branched octane. A comparison of the structure and solvation force using molecular dynamics simulations", *J. Chem. Phys.* **100**, 3276.
[36] Gao, J., Luedtke, W.D. and Landman, U. (1997) "Origins of solvation forces in confined films", *J. Phys. Chem. B* **101**, 4013.
[37] Winkler, R.G. and Hentschke, R. (1993) "Liquid benzene confined between graphite surfaces. A constant pressure molecular dynamics study", *J. Chem. Phys.* **99**, 5405.
[38] Wang, J.-C. and Fichthorn, K.A. (2000) "A method for molecular dynamics simulation of confined fluids", *J. Chem. Phys.* **112**, 8252.
[39] Wang, J.-C. and Fichthorn, K.A. (2002) "Molecular dynamics studies of the effects of chain branching on the properties of confined alkanes", *J. Chem. Phys.* **116**, 410.
[40] Henderson, J.R. (1983) "Potential-distribution theorem: mechanical stability and Kirkwood's integral equation", *Mol. Phys.* **48**, 715.
[41] Schoen, M., Diestler, D.J. and Cushman, J.H. (1994) "Stratification-induced order-disorder phase transitions in molecularly thin confined films", *J. Chem. Phys.* **101**, 6865.
[42] Allen, M.P. and Tildesley, D.J. (1989) *Computer Simulation of Liquids* (Clarendon Press, Oxford).
[43] Berendsen, H.J.C., Postma, J.P.M., van Gunsteren, W.F., DiNola, A. and Haak, J.R. (1984) "Molecular dynamics with coupling to an external bath", *J. Chem. Phys.* **81**, 3684.
[44] Todd, B.D., Evans, D.J. and Daivis, P.J. (1995) "Pressure tensor for inhomogeneous fluids", *Phys. Rev. E* **52**, 1627.
[45] Bordarier, P., Rousseau, B. and Fuchs, A.H. (1997) "Rheology of model confined ultrathin fluid films. I. Statistical mechanics of the surface force apparatus experiments", *J. Chem. Phys.* **106**, 7295.
[46] Fung, Y.C. (1968) *Foundations of Solid Mechanics* (Prentice Hall, Englewood Cliffs, NJ).
[47] Schoen, M., Diestler, D.J. and Cushman, J.H. (1994) "Fluids in micropores. IV. The behavior of molecularly thin confined films in the grand isostress ensembles", *J. Chem. Phys.* **100**, 7707.
[48] Kopsias, N.P. and Theodorou, D.N. (1998) "Elementary structural transitions in the amorphous Lennard–Jones solid using multidimensional transition-state theory", *J. Chem. Phys.* **109**, 8573.
[49] McDonald, I.R. and Singer, K. (1972) "An equation of state for simple liquids", *Mol. Phys.* **23**, 29.
[50] Schoen, M. (1996) "The impact of discrete wall structure on the stratification-induced structural phase transitions in confined films", *J. Chem. Phys.* **105**, 2910.